Feedback Control for the Precise Shape Morphing of 4D-Printed Shape Memory Polymer

Qinglei Ji , Mo Chen, Chun Zhao, Xiran Zhang, Xi Vincent Wang , Lihui Wang , and Lei Feng , *Member, IEEE*

Abstract—**Four-dimensional printing (4DP) is a newly emerged technology that uses smart materials for additive manufacturing and thus enables shape and/or property change upon stimulus after the printing process. Present study on 4DP has been focused on open-loop stimulus, which can hardly ensure high shape precision and predictable final states. In this article, a new closed-loop 4DP (CL4DP) process supplementing 4D printed actuation with closed loop control methods is proposed. Image feedback is used for enhancing the conventional open loop 4DP morphing process and a controller is implemented to regulate the intensity of the stimulus accordingly in real-time. To achieve precise control, a nonlinear affine system model is built by model identification with measurement data to describe the dynamic shape recovery process of the 4D-printed shape memory polymer (SMP). Precise shape control is achieved and the effects of controller parameters on the precision of CL4DP are studied. Traditionally, SMP has a discrete number of selected steady states. With CL4DP, such steady states can be continuous and arbitrary.**

Index Terms—**Closed-loop control, four-dimensional printing (4DP), shape memory polymer (SMP).**

I. INTRODUCTION

FOUR-dimensional printing (4DP) is defined as a prototyping technology that builds 3-D printed structures with smart materials to enable the object morphing under external stimuli [1]–[7]. The technology is foreseen by the yearly Gartner Hype Cycle for Emerging Technologies [8], [9] as one of the most promising technologies that will enjoy a flourishing development in the coming years.

One of the most promising and widely used material for 4DP is shape memory polymer (SMP), which has shape memory effect (SME) with which a material can return from a deformed temporary shape to its original permanent shape via external stimulus [10]–[13]. As shown in Fig. 1(a), typical 4D-printed thermal SMPs have two stable states: permanent shape and temporary shape [4], [14], [15]. Objects are printed with the permanent shape. If heated up above the glass transition temperature T_g, the material is softened and can be deformed into a temporary shape. When cooled down, the temporary shape will be held until the object is heated above T_g again. Then, the heated object recovers the permanent shape and the internal stress is released. However, the conventional SMP recovery suffers from poor precision, poor reproducibility, and unpredictable recovery rate [16]–[18]. Tobushi *et al.* [19] highlighted the issue of irrecoverable strain when SMP is held at a high temperature for a long time and used such strain to obtain new shapes. Singhal *et al.* [20] studied unpredictability of SMP actuation rate and controlled the complete shape recovery time via systematically varied hydrophobicity. Yu *et al.* [21] reported the influence of different SMP programming parameters, such as the programming temperature and the heating time, and proposed a performance map to characterize the shape memory performance. Mather *et al.* [10] reviewed the SMP research progress and highlighted the importance of SMP recovery in a controlled fashion and precisely tailoring the triggering breadth and recovery rate of SMP.

Furthermore, to enable more potential applications, researchers have been striving to increase the number of temporary states of SMPs [22], [23]. Existing methods include increasing the number of discrete reversible phase transitions in the polymer [24]–[28] and tailoring the shape memory transition temperatures [22], [29]–[31]. However, these methods require predesign, preprogramming with good knowledge of a specific material and have limited use cases due to the specifically designed shape recovery scenario.

From control engineering perspective, an open-loop 4DP process is susceptible to many disturbances, such as the following.

1) variation of material property in spatial dimension regarding material distribution or in time dimension regarding variance in different prints;
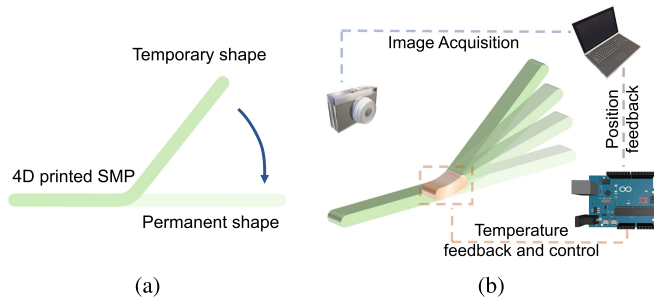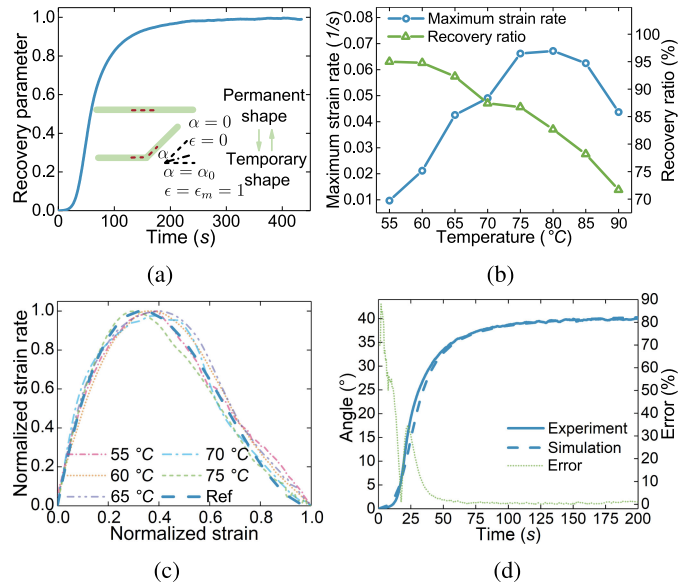
Fig. 1. Two SMP recovery patterns. (a) Typical SMP recovery process. (b) Novel CL4DP process.

Fig. 2. Modeling of SMP recovery. (a) SMP recovery process. The recovery parameter can be any parameter that can describe how much the SMP is recovered such as angle, displacement, and strain. (b) Maximum strain rate and recovery ratio versus temperature. (c) Normalized strain rate versus normalized strain. (d) Comparison between the simulation and experiment results of angle variation during an SMP recovery process with constant temperature stimulus.

2) dimensional error in the 4DP process, which can be caused by low material quality, poor coordination between the material extrusion, and stage displacement;
3) noise in the stimulus, such as the disturbances from the environment and equipment.

Hence, 4DP needs closed-loop monitoring and control to reach high precision. However, few controlled 4DP studies have been investigated. Wang *et al.* [32] developed a novel material, which exhibits relatively better linear relationship between shape recovery and corresponding stress, and thus arbitrary shape changes can be realized by applying this relationship. However, this process is limited with the chosen range of materials. Zolfagharian *et al.* [33] studied the bending control of a 3-D printed polyelectrolyte soft actuator with an uncertain model. In their work, fuzzy subsystems are derived for modeling of the actuator. Then, a sliding mode control law is employed to ensure the stability of the closed-loop fuzzy system and deal with model uncertainties. However, 3-D printing is only applied as a fabrication method for the polyelectrolyte soft actuator. The 3-D printing effects are not studied and it cannot be treated as a 4DP work.

This article designs and implements a closed-loop control strategy to the 4D-printed SMP morphing process, namely closed-loop 4DP (CL4DP) as illustrated in Fig. 1(b). The contributions are the following. A data-driven nonlinear model is developed to describe the dynamic characteristics of the SMP recovery process. A proportional-integral (PI) controller with antiwindup is designed to control the SMP to precisely reach arbitrary temporary states with high repeatability. A self-sensed heating unit is developed to provide fast and precise temperature stimulus for the SMP actuation. The advantage of our method compared to previous results [22], [28], [29] is that the target positions for the SMP to precisely reach are continuous. Influence of 4DP parameters, such as infill direction and mixture ratio on the control result, is studied. As an application of the proposed CL4DP, a small car whose chassis is supported by SMP is fabricated, so that the chassis height can be precisely changed by the CL4DP control method.

This article is organized as follows. The SMP recovery process is modeled in Section II. The build up of the CL4DP system is described in Section III. Section III is divided into three sections. Section III-A introduces the principle and verification of the self-sensed heating unit. Section III-B builds the motion

controller for the SMP recovery process and analyzes the effects of the control parameters. Section III-C studies how model errors affect the control result. The implementation of CL4DP for a small car transformation is elucidated in Section IV. Section V concludes this article.

II. MODELING OF SMP RECOVERY

To achieve a precise control of 4DP, it is necessary to acquire an explicit model of the shape recovery dynamics of the SMP. The study on the characteristics of internal strain and stress of SMP regarding its shape and temperature has been deeply investigated since 2001 [14], [21], [34], [35]. However, these models are not suitable to derive the macroevolution of 4D-printed SMP as they are limited to the static stress–strain relation, which cannot be applied to describe the dynamic movement, such as the recovery velocity variation. Furthermore, the complex infill patterns and printing uncertainties make it even harder to acquire a reliable model for 4D-printed SMP.

In this article, polylactic acid (PLA) and thermoplastic polyurethane (TPU) blends are used for fabricating SMP samples. Fig. 2(a) shows a typical recovery process upon a constant temperature stimulus where the *y*-axis represents the shape recovery characteristics, such as recovered angle, recovered distance, or recovered strain. The recovery speed, which is the derivative of the recovery angle (or strain depending on the legend of the *y*-axis), accelerates at the beginning of the recovery process and then reaches the maximal value in the middle of the process. After the middle point, the recovery speed slows down and SMP continues moving with slower speed until it reaches

the final position. In our study, angles are captured to represent the recovery status. The *recovered angle* α is defined as the angular difference between the measured position and the initial temporary position, as illustrated in Fig. 2(a). The *maximum predeformation angle* (the process of changing the shape of an SMP object from its permanent shape to a temporary shape) is noted as α_0. For simplicity, a dimensionless parameter, *strain*, is defined as the ratio of the recovered angle $\alpha(t)$ and the maximum predeformation angle α_0, represented as follows:

$$\epsilon(t) = \frac{\alpha(t)}{\alpha_0}. \tag{1}$$

Thus, the *strain rate* $\dot{\epsilon}(t)$, as the derivative of $\epsilon(t)$ to time, represents how fast the SMP is recovering to its permanent shape. The *maximum strain rate* representing the maximum recovery angular speed for a recovery process is noted as $\dot{\epsilon}_m(T)$, which is dependent on the temperature stimulus T. The blue line of Fig. 2(b) shows the variation of the maximum strain rate $\dot{\epsilon}_m(T)$ for different temperatures. For temperature in the range of $[55\,°C,\ 75\,°C]$, $\dot{\epsilon}_m(T)$ is approximately a linear increase with the temperature input, which can be expressed as follows:

$$\dot{\epsilon}_m(T) = aT + b \tag{2}$$

where $a = 0.0028$ and $b = -0.1454$. Assuming that the relation is still linear for lower temperatures and let $\dot{\epsilon}_m(T) = 0$, the *critical temperature* $T_c = -b/a$ is acquired, which indicates the temperature under which the strain rate is always zero and recovery cannot happen. In this article, $T_c = 52\,°C$. In the temperature range of $[55\,°C,\ 75\,°C]$, the strain rate $\dot{\epsilon}(t)$ for different temperatures can be normalized with the maximum strain rate $\dot{\epsilon}_m(T)$ and the *normalized strain rate* is the following:

$$\bar{\dot{\epsilon}}(t, T) = \frac{\dot{\epsilon}(t)}{\dot{\epsilon}_m(T)} = \frac{\dot{\epsilon}(t)}{aT + b} \tag{3}$$

where $\bar{\dot{\epsilon}}(t, T)$ varies between 0 and 1.

Previous study has found that the SMP cannot recover completely to its permanent shape [36], [37] and this difference can be described by the *recovery ratio* $R_r = \frac{\alpha(\infty)}{\alpha_0}$, where $\alpha(\infty) = \lim_{t \to \infty} \alpha(t)$ is the final recovered angle. The limit must exist because the shape recovery process is irreversible and $\alpha(t)$ cannot be larger than α_0. According to (1), $R_r = \epsilon(\infty)$. The recovery ratio is affected by the materials composition, predeformation temperature, and recovery temperature. The green line in Fig. 2(b) shows the relation between the recovery ratio and different temperature stimulus when the same temperature is used for predeformation and recovery stimulus. In the temperature range of $[55\,°C,\ 75\,°C]$, R_r shows small difference around $R_r = 90\%$, but drops largely after $80\,°C$.

As aforementioned, the maximum value of strain equals the recovery ratio. Thus, the strain can be normalized using the recovery ratio R_r as follows:

$$\bar{\epsilon}(t) = \frac{\epsilon(t)}{R_r} \tag{4}$$

where $\bar{\epsilon}$ is the normalized strain and varies from 0 to 1. In temperature range $[55\,°C,\ 75\,°C]$, the same recovery ratio $R_r = 0.9$ is applied for the normalization: $\bar{\epsilon} = \epsilon/0.9$.

Normalized strain rate $\bar{\dot{\epsilon}}$ is plotted versus normalized strain $\bar{\epsilon}$ for different temperatures, as shown in Fig. 2(c). The figure indicates that (a) the normalized strain rate reaches the peak value of 1 at around one-third of the total recovery process and (b) decreases to 0 at the end (c) with a zero acceleration so that the morphing process can stop. Together with the condition that (d) the curve must pass the origin, these four boundary conditions mean that the curve can be described with a third-order polynomial

$$\bar{\dot{\epsilon}}(t, T) = 6.75\bar{\epsilon}(t)(\bar{\epsilon}(t) - 1)^2. \tag{5}$$

With (3)–(5), in the temperature range $[55\,°C,\ 75\,°C]$, the following relation is acquired:

$$\dot{\epsilon}(t) = 6.75 \times \frac{\epsilon(t)}{R_r}\left(\frac{\epsilon(t)}{R_r} - 1\right)^2 (aT + b). \tag{6}$$

Equation (6) describes a nonlinear affine system model. a, b, and R_r are constants related to the SMP property and stimulus range. Variables ϵ and T represent the system state variable and system input, respectively. Using (1), the model can now be more explicitly described as

$$\dot{\alpha}(t) = 6.75 \times \frac{\alpha(t)}{R_r}\left(\frac{\alpha(t)}{\alpha_0 R_r} - 1\right)^2 (aT + b) \tag{7}$$

where T is the temperature input, α_0 is the predeformation angle, and $\alpha(t)$ and $\dot{\alpha}(t)$ are the recovered angle and the recovered angular speed, respectively. a, b, and R_r are constants related to the SMP as mentioned previously. For the modeling of SMP recovery in our study, temperature stimulus tests are performed three times for the predeformation angle α_0 of $45°, 77.5°$, and $90°$. These nine groups of data are then averaged for acquiring the model. In one test case where $T = 55\,°C$ and $\alpha_0 = 45°$, the response of $\alpha(t)$ can be estimated by (7). Fig. 2(d) shows the experimental and simulated results of the variation of the angle versus time. The green line shows that the error is up to 90% at the beginning and converges to zero in the end.

III. PRECISE SHAPE CONTROL FOR SMP

With the aforementioned model, the SMP shape morphing can be regulated precisely to a middle state by changing the stimulus temperature during the 4DP morphing process rather than always recovering to the permanent shape. The control loop is illustrated in Fig. 3(a). Two controllers are implemented in a cascade structure to achieve temperature control and morphing control, respectively, as shown in Fig. 3(b) and (c). The difference between the position reference and the real position is first calculated and sent to the morphing controller. The controller then sends out a reference temperature value in order to achieve the target position. The temperature reference is then compared with the real temperature of the heating unit and the temperature difference is received by the temperature controller. The temperature controller calculates the required electric voltage to achieve the target temperature. This voltage reference signal is then read by a power supply and applied to the heating circuit to heat the SMP and regulate the morphing process.
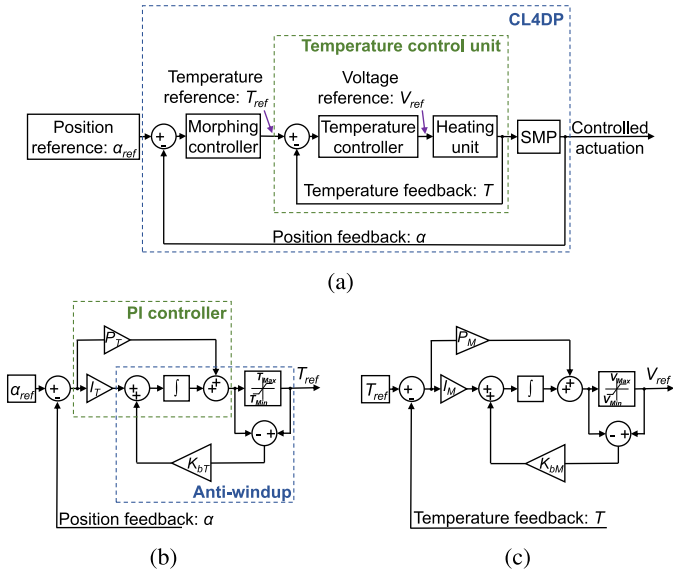
Fig. 3. Closed-loop control set-up for CL4DP. (a) Cascade control structure of the CL4DP. (b) Temperature controller. (c) Morphing controller structure.
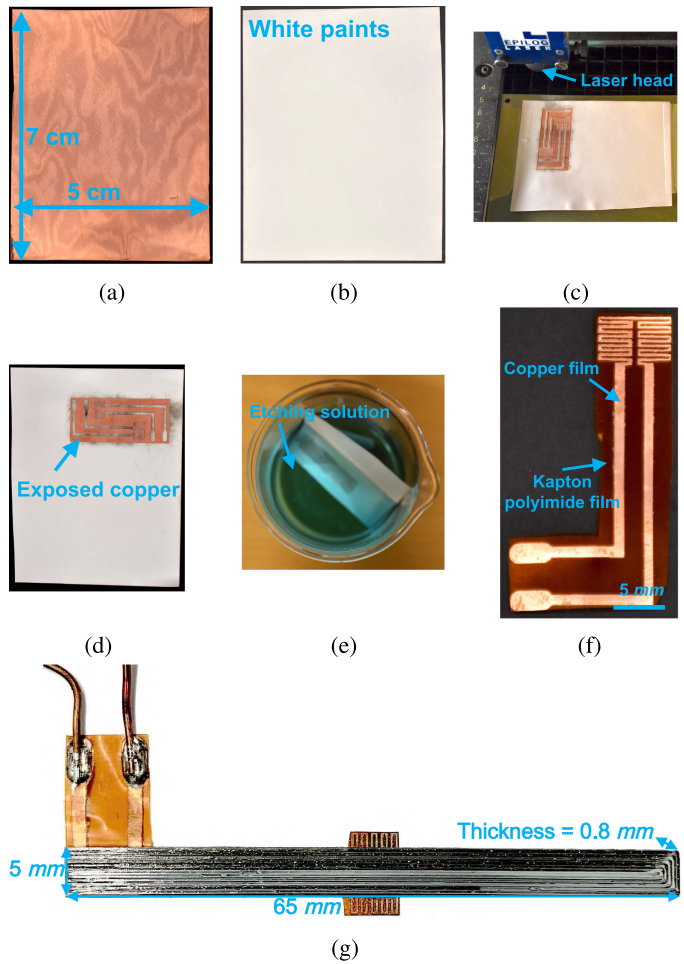

Fig. 4. Fabrication of the heating circuit. (a) Copper film. (b) Cover the copper film with white paints. (c) Use laser beam to carve the paints. (d) Exposed copper after laser carving. (e) Etch the exposed copper. (f) Fabricated heating circuit. (g) Heating circuit is stuck to the SMP.

A. Precise Temperature Stimulus With a Self-Sensed Heating Circuit

Traditional heating devices have a separate heating source and a sensor for temperature monitoring, which are not portable and hard to implement for the SMP stimulus. This study develops a tiny heating unit that can self-sense its temperature to realize fast-response and controllable temperature.

The heating circuit is fabricated with a single-sided Pyralux flexible copper laminate, which is made of a composite Kapton polyimide film with copper foil on one side as shown in Fig. 4(a). The Kapton base is $50\,\mu$m and the copper base is $30\,\mu$m. The laminate is then covered with spray paint that evaporates under high temperature over around $200\,°$C, as shown in Fig. 4(b). The circuit is designed with Adobe Illustrator and then loaded to a 75-W Epilog Fusion laser cutter, which is shown in Fig. 4(c). The laser beam travels over the painted copper film and locally heats the unwanted copper positions. As a result, the local paints vaporize and the covered copper under the evaporated paints is exposed to air, which is marked in Fig. 4(d). The entire film is then immersed in $70\,°$C etching solution (sodium persulfate) for 30 min to fully dissolve the exposed copper as shown in Fig. 4(e). After etching, the useless areas are cut out and the heating areas are remained as shown in Fig. 4(f). Fig. 4(g) shows that the heating circuit is attached to the SMP.

The copper has resistance coefficient that is linear to temperature [38]. The relation can be expressed as

$$R(T) = R_{\text{ref}}[1 + \kappa(T - T_{\text{ref}})] \qquad (8)$$

where R_{ref} represents the electric resistance at a reference temperature T_{ref} and κ is the temperature coefficient of resistance for the material. Here, $T_{\text{ref}} = 20\,°$C and $\kappa_{\text{copper}} = 0.00393$. $R(T)$ is the resistance at temperature T. With (8), the temperature of the copper circuit can be estimated with the real-time resistance

$$T(R) = \frac{1}{\kappa}\left(\frac{R}{R_{\text{ref}}} - 1\right) + T_{\text{ref}}. \qquad (9)$$

The electric resistance of the heating circuit is calculated using Ohm's law with the measured electric voltage and current and then (9) is applied to calculate the real-time temperature of the heating circuit.

Step response tests are performed to acquire the temperature response model of the heating circuit. Electric voltage of 0.2–1 V with a step of 0.1 V is applied on the heating circuit and the temperature responses are recorded and normalized with the squared value of the corresponding voltage as shown in Fig. 5(a). It is found that the *normalized temperature* responses under different electric voltages are basically the same. These responses are then averaged and fitted with *tfest* function in MATLAB to acquire the transfer function between the normalized temperature and the *squared electric voltage*. The transfer function can be expressed
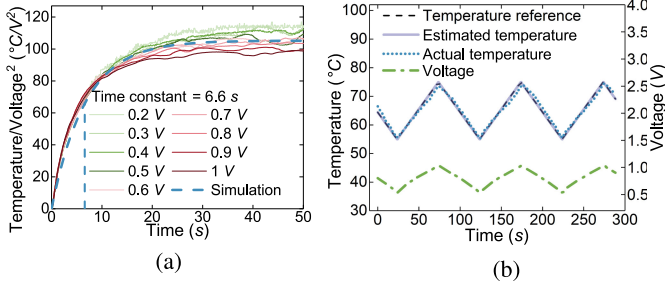
Fig. 5. Temperature response and control. (a) Normalized temperature response under different electric voltage inputs. (b) Calibration of temperature.

as

$$\frac{T(z)}{U(z)} = \frac{bz^{-1}}{1 - az^{-1}} \qquad (10)$$

where T represents the normalized temperature over the square of the voltage and U represents the square of the voltage. $a = 0.9926$ and $b = 0.7818$. Discrete time of the system is $T_s = 0.05$ s.

With the model, a PI controller with antiwindup is applied for controlling the temperature precisely and rapidly. The structure of the controller is illustrated in Fig. 3(b). Once a required temperature is given as the reference, the controller will calculate the applied electric voltage automatically to regulate the actual temperature to the reference value. The autotuning function in MATLAB Simulink is used with the aforementioned heating circuit model to tune the controller parameters to meet the following requirements: no overshoot to avoid fusion of the material or burning of the heating circuit; and rise time should be as short as possible to provide quick temperature stimulus for the SMP. A fine-tuned PI controller with antiwindup satisfying these requirements is then implemented on the temperature control unit. The parameters used for the temperature controller is as follows: $P_T = 0.3$, $I_T = 0.2$, and $K_{bT} = 6$. The electric voltage limits are: $V_{\min} = 0.2$ V to ensure that there is always current in the circuit so that the resistance of the circuit can be calculated, and $V_{\max} = 0.9$ V to ensure a maximum heating temperature around $80\,°C$ for protecting the SMP.

To test the controller experimentally, the temperature reference is set to vary in the temperature range of $[55\,°C, \ 75\,°C]$, which is the temperature range that the SMP model in the main text functions. The electric voltage and current of the heating circuit are measured with an INA219 High Side DC Current Sensor Breakout that is connected with the heating circuit. The voltage source of the circuit is an RND 320-KD3005P Programmable Bench Top Power Supply (RND Lab) and controlled in real time with an Arduino Mega 2560 board. The aforementioned estimated temperature from the electric resistance is provided to the controller as the temperature feedback. As shown in Fig. 5(b), the estimated temperature using the electric resistance follows the temperature reference well. The error between the actual temperature (measured with an independent thermal camera) and the estimated temperature from the electric resistance is

always lower than 5%, which further proves the feasibility of the temperature estimation with electric resistance. The maximum time delay for the actual temperature to meet the temperature reference is smaller than 2 s, which is more than ten times faster than the SMP response time. So, it is reasonable to use the cascade controller. The corresponding voltage trajectory is shown with the green line.

B. Effects of Motion Control Parameters

A Logitech c270 webcamera is used to capture the morphing at 30 frames per second (fps) and images are analyzed in Python running on a computer to estimate the real-time angle feedback. The acquired angle is sent to an Arduino Mega 2560 board, which performs control functions. Fig. 3(c) shows a PI controller structure designed for the nonlinear SMP model with MATLAB Simulink. An antiwindup function and output saturation are also used to limit the controlled temperature in the functional temperature range $[55\,°C, \ 75\,°C]$. The controller changes the temperature in real time according to the instant position to meet the control target. To acquire an expected controller, the effects of the morphing controller parameters including the proportional value P_M, the integral value I_M, and the back-calculation coefficient K_{bM} shown in Fig. 3(c) on the control results will be studied.

The rise time and the static error are used to evaluate the control performance. The rise time is defined as the time length of the control process from 5 to 95% of the position reference. The static error is defined as the error between the controlled position and the position reference at 200 s. Fig. 6(a) shows the effect of various P_M values on the static error and rise time while fixing $I_M = 2$ and $K_{bM} = 1$. The static error rapidly approaches zero when P_M increases and equals zero when P_M is around 50. On the other hand, the rise time decreases a little bit for small P_M and then increases almost linearly with P_M.

Furthermore, the influence of the I_M value is studied. If P_M is fixed at 50 and K_{bM} still equals 1, the static error decreases rapidly and then reaches zero at around $I_M = 2$, as shown in Fig. 6(b). The rise time decreases for increasing I_M. Finally, if $P_M = 50$ and $I_M = 2$, the increase in K_{bM} will slightly increase the rise time and increase the static error as shown in Fig. 6(c). Note that the static error is always above 0 as the SMP recovery is not reversible such that the final angle is always slightly larger than the reference.

A group of control parameters that minimize the static error are picked to perform the CL4DP: $P_M = 50$, $I_M = 2$, and $K_{bM} = 1$. Fig. 6(d) shows the angle changing process with angle references as $15°$, $22.5°$, and $30°$. The predeformed angle α_0 is $45°$. The bottom plots in Fig. 6(d) show the corresponding temperature stimulus. It is found that the correspondence between the experiment and simulation results differs for different control references, as shown in Fig. 6(e). To describe this correspondence quantitatively, two variables are defined. The *difference of rise time* refers to the difference between the rise time $t_{\exp}$ in the experiments and the rise time t_{sim} from simulation with the same control reference of the experiments. It is calculated by: $(t_{\exp} - t_{\text{sim}})/t_{\text{sim}}$. The *difference of static*
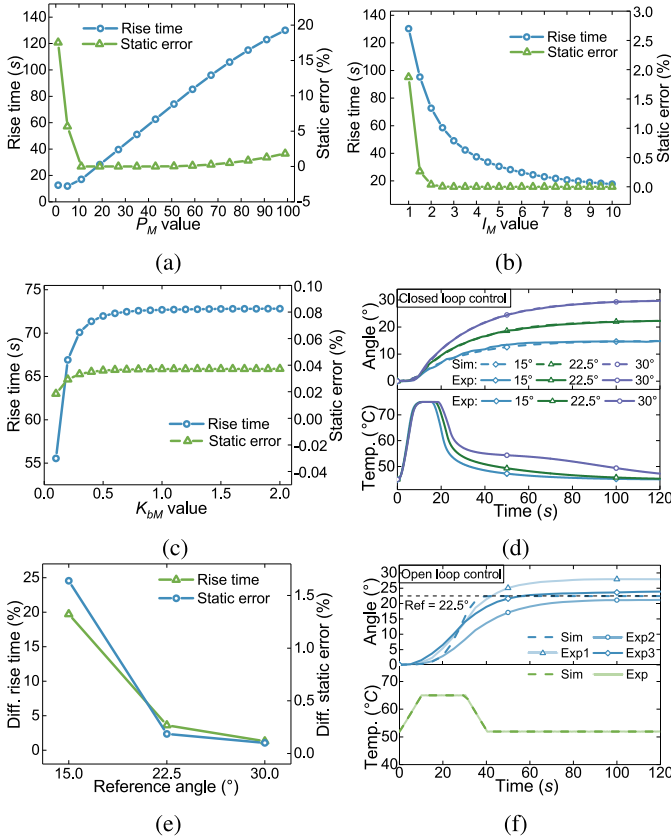
Fig. 6. CL4DP. (a) Effects of P_M value on the rise time and static error at 200 s. (b) Effects of I_M value on the rise time and static error at 200 s. (c) Effects of K_{bM} value on the rise time and static error at 200 s. (d) Angle variation when controlling different final positions. (e) Influence of reference angles on the control result. (f) Open-loop control results.

error is defined as the difference between the static error e_{exp} of experiments and static error e_{sim} of simulation with the same control reference of the experiments. It is calculated with: $(e_{exp} - e_{sim})/e_{sim}$. The difference of rise time is up to 20% for small reference angles and tends to zero when the position reference is larger than half of the maximum predeformation. The difference of static error is always around zero for all control targets and is smaller for larger reference targets.

The closed-loop control results are then compared with open-loop control. The control data with a reference of 22.5° are used for the comparison. The temperature stimulus for the open-loop process is illustrated in the bottom of Fig. 6(f) and can be expressed as

$$T(t) = \begin{cases} 1.3t + 52, & 0\,\text{s} \leq t < 10\,\text{s} \\ 65, & 10\,\text{s} \leq t < 30.2\,\text{s} \\ -1.3t + 104.26, & 30.2\,\text{s} \leq t < 40.2\,\text{s} \\ 52, & t \geq 40.2\,\text{s} \end{cases}. \quad (11)$$

The open-loop controller exactly reaches 22.5° in simulation. However, as shown in Fig. 6(f), in the three experiment tests that are performed, the final angles all failed to stop at the reference angle. The angle errors for the three open-loop tests are 24%,

6.2%, and 5.8%, respectively, while the error of closed-loop control is only 0.8%, which proves the precision of CL4DP.
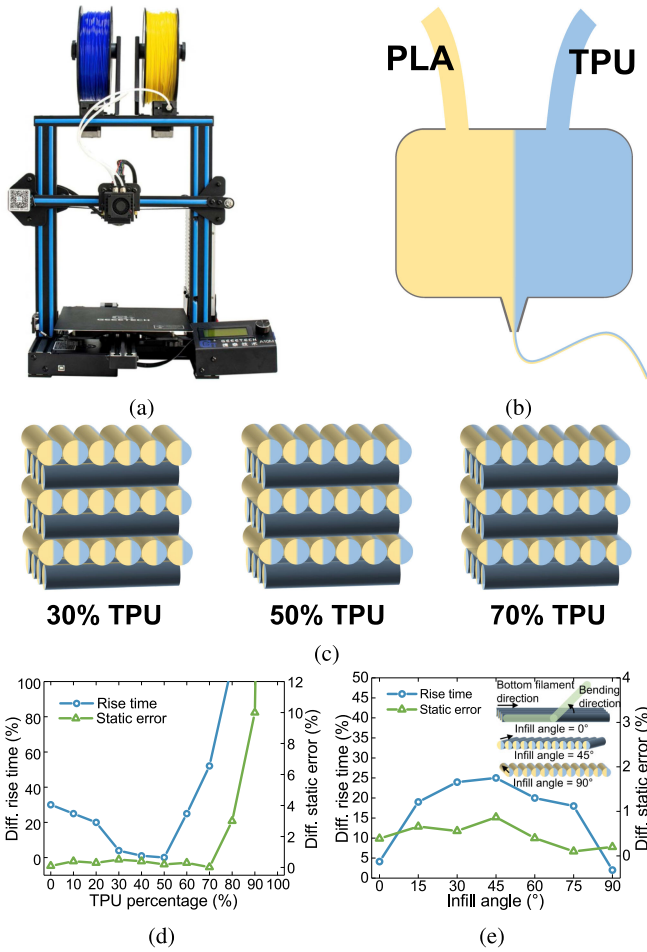
C. Effects of Model Error

The composition and printing methods of the SMP also affect the control result. The same control strategy is used while varying the SMP fabrication parameters in order to investigate their effect. Two main factors studied are the material composition and the infill angle during the printing process. Their effect on the control result are studied by comparing the experiment results with the simulation results.

The disturbance in the material composition is first studied. Blends of PLA and TPU are applied in this article for higher recovery rate. PLA is a commonly used 3-D printing material featured with good printability and utility. PLA shows SME and has a glass transition temperature $T_g = 55\,°\text{C}$ and melting temperature $T_m = 180\,°\text{C}$. Traditional methods of mixing the material and then fabricating with the blends are time consuming and require professional material operation experience. However, 4DP technology enables to print these two materials with different mix ratios in one print. A Geeetech A10M mix-color 3-D printer shown in Fig. 7(a) is used for printing. The printer can simultaneously feed PLA and TPU filaments (PrimaSelect, both provided by 3D Prima) and heat the materials in the same chamber until they are extruded and form a filament combining these two materials as shown in Fig. 7(b). Fig. 7(c) shows a typical cross section of prints with 70% PLA and 30% TPU, 50% PLA and 50% TPU, and 30% PLA and 70% TPU. The sample with 50% PLA and 50% TPU is regarded as the standard composition for modeling. The glass transition temperature of the standard sample is 52 °C and the rise time (defined as the time length of the recovery process from 5 to 95% of the final position upon a constant temperature stimulus of 65 °C) is 73.7 s. The failure stress and strain are 7.8 MPa and 1.28%, respectively.

Here, we use the content percentage of TPU to describe the disturbance as shown in Fig. 7(d). The blue line shows that when the percentage of TPU increases from 0 to 100%, the difference of rise time decreases from a positive error around 30% to zero when the material is identical to the standard composition. The difference of rise time increases rapidly for larger TPU percentage and approaches positive infinity for 100% TPU. At this point, the material exhibits no SME and is totally elastic so that the rise time for the material to recover to the permanent position is almost zero. The green line in Fig. 7(d) shows that the difference of static error is almost the same as zero for TPU percentage up to 75% while it increases to positive infinity when TPU percentage approaches 100%. As a conclusion, the rise time is influenced by the compositional variant obviously. The static error of the controller shows good robustness as long as the material still shows SME.

The infill angles during the 4DP process also influence the control result. The inset of Fig. 7(e) shows the different values of infill angles during printing. The infill angle represents the printed filament direction of the first printed layer, which also gives an indication of the distributions of the materials in the other layers as the filament directions for two neighbor layers
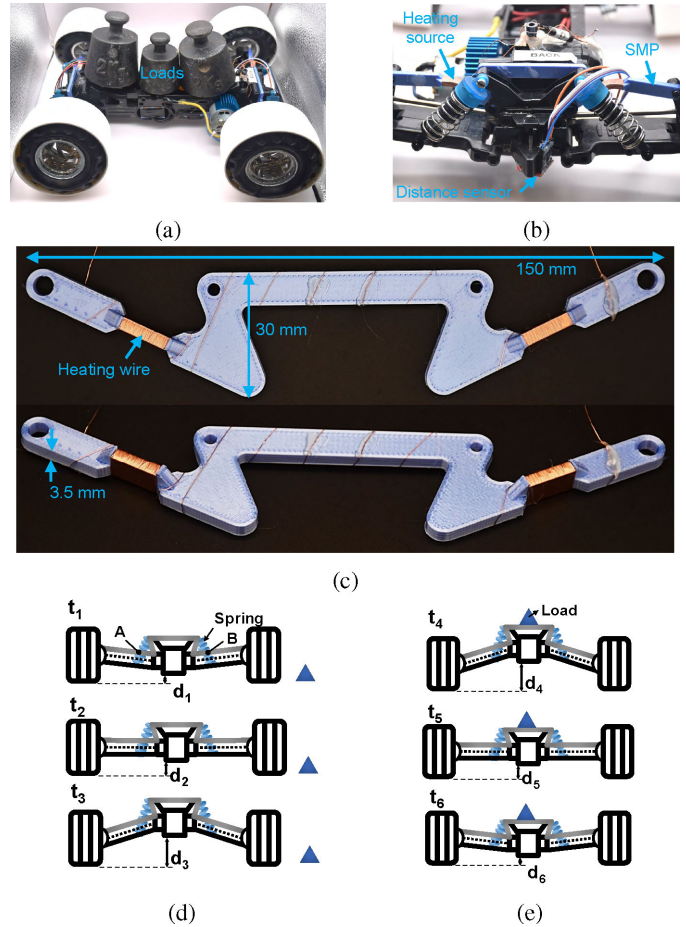
Fig. 7. 4DP of SMP with controllable composition and effects of model errors. (a) Geeetech A10M mix-color 3-D printer for mixing and printing the SMP with different compositions and infills. (b) Schematic of the mixing extruder. (c) Schematic of printed sample with different material compositions. (d) Effects of material composition (TPU percentage) on the rise time and static error of control results. (e) Effects of infill angles during 3DP on the rise time and static error of control results.

Fig. 8. Height control design of the small car chassis. (a) Front view of the small car. (b) Components of the small car. (c) SMP frame with heating wires. (d) Ascending of the small car. (e) Descending of the small car.

are perpendicular to each other. The infill angle of $0°$ is defined as the printing direction along the long side of the printed SMP and $90°$ defines that the printing direction is perpendicular to the long side. As shown by the blue line in Fig. 7(e), while the infill angle during 4DP increases from $0°$ to $45°$, the difference of rise time increases to a maximum value around 25%. When the infill angle further increases from $45°$ to $90°$, the variation of the difference of rise time is approximately symmetric to $45°$. The green line shows that the difference of static error is almost zero for all infill angles and is also approximately symmetric to $45°$.

## IV. APPLICATION: SMALL CAR TRANSFORMATION ENABLED WITH CL4DP

In this section, a small car prototype is introduced to demonstrate the potential application of CL4DP. Modern vehicles use suspension systems to change body height, which require complex mechanisms. Here, the support structure of a small car

is replaced by the previously mentioned SMP material, which is able to vary its shape continuously in a range through CL4DP method as shown in Fig. 8(a) and (b). Fig. 8(c) shows the front SMP frame structure as an example. Two gaps are designed for hosting the copper wire and baffle plates are used for fixing the edges of the heating wire to avoid free movement.

As illustrated in Fig. 8(d), the printed SMP frame is in its permanent shape that keeps the small car in its lowest position at time t_1. Positions A and B of the frame are surrounded by copper wires that provide heating power to regulate temperature. Two springs are mounted to balance the gravity and are compressed at the lowest position so that they can lift the small car to the highest position when the SMP is heated. At low temperature, the SMP frame is rigid enough to counterbalance the spring force and hence fixes the car chassis in its lowest state. At this point, the center of gravity of the small car is also the lowest, which makes the small car stable and suitable to run in high speed. However, when heating positions A and B up to temperature T_g of the material, the SMP becomes soft and the spring force now lifts the car as shown at time t_2 until the highest point. When the transformation stops, the temperature decreases and the frame
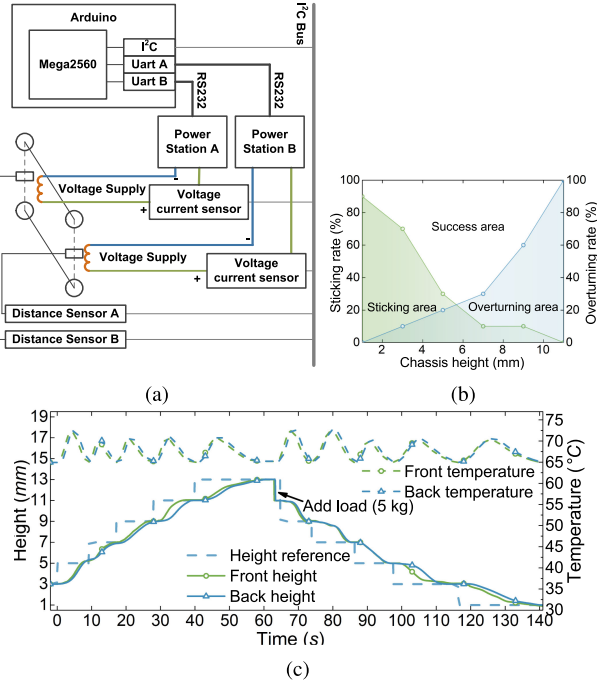
Fig. 9. Height control results. (a) Schematic of the height control system for the small car. (b) Influence of the small car chassis height on the overturning rate and the sticking rate. (c) Height control.

becomes hard again at t_3 so that the small car is fixed in a higher position while the SMP is in its temporary shape. The gravity center and the small car chassis height are high now, which is suitable for low speed driving and bumpy roads.

To make the shape transformation repeatable, a load of 5 kg is mounted on the small car to increase the body weight so that the gravity and the shape memory force can cooperate to overcome the spring force, which enables the chassis to recover to the lowest position upon heating the SMP again as shown in Fig. 8(e) at time t_4 and t_5. The temperature then goes down at t_6 and the load is unloaded. The state is now returned to t_1 and the transformation process can repeat when the temperature goes up again.

In our design, the aforementioned process is controlled with CL4DP method. The small car height control system has two independent height control loops that share the same control board as shown in Fig. 9(a). An Arduino Mega 2560 is applied as the control board and the I^{2}C bus is used for the signal acquisition from the two distance sensors for the front and back chassis heights and two voltage–current sensors for calculating the electric resistance. The information is then analyzed with the CL4DP controller and the reference voltage values are sent to the power stations. The heating elements are then heated up so that the SMP starts to change the heights under the feedback control, which enables the height of the small car to be adjusted to any value between the lowest and the highest positions.

Similar to Section II, the control starts with the model describing the chassis height response under different temperatures. Following the same experiment and data processing methods, similar model, as (5) that describes the dynamics of the height

changing process, can be applied and expressed explicitly as

$$v(t) = 6.75 \times \frac{h(t)}{h_0} \left(\frac{h(t)}{h_0} - 1 \right)^2 (mT + n) \qquad (12)$$

where $v(t)$ is the height change speed, $h(t)$ is the real-time height, $h_0 = 10$ mm is the height variation range mentioned earlier, T is the temperature over the SMP, $m = 0.0449$ mm/s $\cdot°$C, and $n = -2.8356$ mm/s. Similar to CL4DP, a PI controller with antiwindup is applied for height control. The controller parameters are redesigned using the new model parameters. The new control parameters are $P = 3$, $I = 0.02$, and $K_b = 1$ and temperature is limited under $85°$C. Fig. 9(c) shows the height control for an ascent process from 3 to 13 mm and a descent process from 11 to 1 mm with a gap height of 2 mm. Notice that there is a height drop of 2 mm when adding the load, which results from the structure deformation of the small car. The small car with different chassis height is then tested on a bumpy road with speed around 0.5 m/s. For lower chassis height, the small car has larger possibility to be stopped by the barriers on the road without turning over and this probability is evaluated with the *sticking rate*, which is the ratio between the number of stops and the total test number. For higher chassis height, the small car tends to turn over and is not stable, because the center of gravity is high. This probability is evaluated with the *overturning rate*, which is the ratio of the number of turning over and the total test number. For each height, ten tests are performed to calculate the overturning rate and sticking rate. Fig. 9(b) demonstrates that higher chassis height results in higher overturning rate and lower sticking rate and vice versa.

V. CONCLUSION

This article elaborated a nonlinear model of the SMP morphing process. Compared with previous SMP models, the proposed model focused on the dynamic recovery process. Since the dynamics of the SMP morphing process was difficult to model by physics, we used a data-driven modeling method to identify the complex nonlinear model through experiments. The contribution in this aspect was to select the proper signals to reveal the hidden relationship between them. Implementation of a closed-loop control for the 4D-printed SMP overcame the inherent drawbacks of SMP. The control strategy enabled this morphing process to be regulated precisely with arbitrary shapes as expected. Compared with open-loop results, CL4DP achieved precise final shapes through feedback control. Model errors caused during the 4DP process were also investigated. Precise and robust control results were observed. A self-sensed heating unit was developed to provide a lightweight and easy-to-implement heating source, which was not only essential for this study, but could also be applied in other thermal stimulated actuations.

A small car, structured by SMP, was printed and the height of the center of gravity of the vehicle could be precisely controlled to change its cross-obstacle ability. This demonstrated the future application of our proposed model and closed-loop control method.

Some problems that are worthy to be further investigated in the future research are concluded as follows.

1) *System consistency*. The SMP cannot always recover to its original permanent shape as the number of repetitions increases. The relationship between the recovery rate and the repeated times along with other environmental factors needs to be studied to build a more accurate model.

2) *System linearity*. As mentioned in the main content, the system is not perfectly linear under different step inputs. The exact model can be further built according to more identification data. Advanced control strategy can be developed to realize better control precision and robustness.

3) *New material development*. The SMP recovery force is normally small and hence limits its wider application. New materials that offer large actuation force can be investigated.

4) *Applications*. Practical applications contributing to the production or medical usage will be explored.

REFERENCES

[1] X. Kuang, K. Chen, C. K. Dunn, J. Wu, V. C. Li, and H. J. Qi, "3D printing of highly stretchable, shape-memory, and self-healing elastomer toward novel 4D printing," *ACS Appl. Mater. Interfaces*, vol. 10, no. 8, pp. 7381–7388, 2018.

[2] Z. Jiang, R. Shaha, K. Jiang, R. McBride, C. Frick, and J. Oakey, "Composite hydrogels with controlled degradation in 3D printed scaffolds," *IEEE Trans. Nanobiosci.*, vol. 18, no. 2, pp. 261–264, Apr. 2019.

[3] C. de Marco, S. Pané, and B. J. Nelson, "4D printing and robotics," *Sci. Robot.*, vol. 3, no. 18, pp. 287–294, 2018.

[4] Y. Y. C. Choong, S. Maleksaeedi, H. Eng, J. Wei, and P. C. Su, "4D printing of high performance shape memory polymer using stereolithography," *Mater. Des.*, vol. 126, pp. 219–225, 2017.

[5] A. Zolfagharian, A. Z. Kouzani, S. Y. Khoo, I. Gibson, and A. Kaynak, "3D printed hydrogel soft actuators," in *Proc. IEEE Region 10 Conf.*, 2016, pp. 2272–2277.

[6] X. Li, J. M. Zhang, X. Yi, Z. Huang, P. Lv, and H. Duan, "Multimaterial microfluidic 3D printing of textured composites with liquid inclusions," *Adv. Sci.*, vol. 6, 2019, Art. no. 1800730.

[7] R. L. Truby and J. A. Lewis, "Printing soft matter in three dimensions," *Nature*, vol. 6, no. 3, 2019, Art. no. 1800730.

[8] M. J. Walker, B. Burton, and M. Cantara, "Hype cycle for emerging technologies," Gartner, Stamford, CT, USA, 2018, pp. 1–73.

[9] X. Kuang *et al.*, "Advances in 4D printing: Materials and applications," *Adv. Funct. Mater.*, vol. 29, no. 2, 2019, Art. no. 1805290.

[10] P. T. Mather, X. Luo, and I. A. Rousseau, "Shape memory polymer research," *Annu. Rev. Mater. Res.*, vol. 39, pp. 445–471, 2009.

[11] L. Hines, V. Arabagi, and M. Sitti, "Shape memory polymer-based flexure stiffness control in a miniature flapping-wing robot," *IEEE Trans. Robot.*, vol. 28, no. 4, pp. 987–990, Aug. 2012.

[12] N. Besse, S. Rosset, J. J. Zarate, E. Ferrari, L. Brayda, and H. Shea, "Understanding graphics on a scalable latching assistive haptic display using a shape memory polymer membrane," *IEEE Trans. Haptics*, vol. 11, no. 1, pp. 30–38, Jan.–Mar. 2018.

[13] A. Bellini, M. Colli, and E. Dragoni, "Mechatronic design of a shape memory alloy actuator for automotive tumble flaps: A case study," *IEEE Trans. Ind. Electron.*, vol. 56, no. 7, pp. 2644–2656, Jul. 2009.

[14] H. Tobushi, K. Okumura, S. Hayashi, and N. Ito, "Thermomechanical constitutive model of shape memory polymer," *Mech. Mater.*, vol. 33, no. 10, pp. 545–554, 2001.

[15] A. Firouzeh, M. Salerno, and J. Paik, "Stiffness control with shape memory polymer in underactuated robotic origamis," *IEEE Trans. Robot.*, vol. 33, no. 4, pp. 765–777, Aug. 2017.

[16] S. A. Madbouly and A. Lendlein, "Shape-memory polymer composites," in *Shape Memory Polymers*. New York, NY, USA: Springer, 2009, pp. 41–95.

[17] N. Nikdel, P. Nikdel, M. A. Badamchizadeh, and I. Hassanzadeh, "Using neural network model predictive control for controlling shape memory alloy-based manipulator," *IEEE Trans. Ind. Electron.*, vol. 61, no. 3, pp. 1394–1401, Mar. 2014.

[18] H. Yang, M. Xu, W. Li, and S. Zhang, "Design and implementation of a soft robotic arm driven by SMA coils," *IEEE Trans. Ind. Electron.*, vol. 66, no. 8, pp. 6108–6116, Aug. 2019.

[19] H. Tobushi, S. Hayashi, K. Hoshio, and Y. Ejiri, "Shape recovery and irrecoverable strain control in polyurethane shape-memory polymer," *Sci. Technol. Adv. Mater*, vol. 9, 2008, Art. no. 015009.

[20] P. Singhal *et al.*, "Controlling the actuation rate of low-density shape-memory polymer foams in water," *Macromol. Chem. Phys*, vol. 214, no. 11, pp. 1204–1214, 2013.

[21] K. Yu, Q. Ge, and H. J. Qi, "Reduced time as a unified parameter determining fixity and free recovery of shape memory polymers," *Nat. Commun.*, vol. 5, no. 1, pp. 1–9, 2014.

[22] T. Xie, "Tunable polymer multi-shape memory effect," *Nature*, vol. 464, no. 7286, pp. 267–270, 2010.

[23] L. Sun and W. M. Huang, "Mechanisms of the multi-shape memory effect and temperature memory effect in shape memory polymers," *Soft Matter*, vol. 6, no. 18, pp. 4403–4406, 2010.

[24] M. Behl, I. Bellin, S. Kelch, W. Wagermaier, and A. Lendlein, "One-step process for creating triple-shape capability of AB polymer networks," *Adv. Funct. Mater.*, vol. 19, no. 1, pp. 102–108, 2009.

[25] T. Xie, X. Xiao, and Y.-T. Cheng, "Revealing triple-shape memory effect by polymer bilayers," *Macromol. Rapid Commun.*, vol. 30, no. 21, pp. 1823–1827, 2009.

[26] P. Prathumrat, S. Tiptipakorn, and S. Rimdusit, "Multiple-shape memory polymers from benzoxazine–urethane copolymers," *Smart Mater. Struct.*, vol. 26, no. 6, 2017, Art. no. 065025.

[27] R. Guseinov, C. McMahan, J. Pérez, C. Daraio, and B. Bickel, "Programming temporal morphing of self-actuated shells," *Nat. Commun.*, vol. 11, no. 1, pp. 1–7, 2020.

[28] X. Hu *et al.*, "Programming temporal shapeshifting," *Nat. Commun.*, vol. 7, no. 1, pp. 1–7, 2016.

[29] T. Xie and I. A. Rousseau, "Facile tailoring of thermal transition temperatures of epoxy shape memory polymers," *Polymer*, vol. 50, no. 8, pp. 1852–1856, 2009.

[30] Y. Liu, B. Shaw, M. D. Dickey, and J. Genzer, "Sequential self-folding of polymer sheets," *Sci. Adv.*, vol. 3, no. 3, 2017, Art. no. e1602417.

[31] A. Basit, G. L'Hostis, and B. Durand, "Multi-shape memory effect in shape memory polymer composites," *Mater. Lett.*, vol. 74, pp. 220–222, 2012.

[32] Y. Wang, Y. Pan, Z. Zheng, and X. Ding, "Thermadapt shape memory polymers with predictable and arbitrary shape shifting," *Macromol. Chem. Phys.*, vol. 220, no. 2, 2019, Art. no. 1800390.

[33] A. Zolfagharian, A. Z. Kouzani, M. Maheepala, S. Y. Khoo, and A. Kaynak, "Bending control of a 3D printed polyelectrolyte soft actuator with uncertain model," *Sensors Actuators, A*, vol. 288, pp. 134–143, 2019.

[34] M. Behl, K. Kratz, U. Noechel, T. Sauter, and A. Lendlein, "Temperature-memory polymer actuators," *Proc. Natl. Acad. Sci. USA*, vol. 110, no. 31, pp. 12555–12559, 2013.

[35] K. Yu, A. J. McClung, G. P. Tandon, J. W. Baur, and H. J. Qi, "A thermomechanical constitutive model for an epoxy based shape memory polymer and its parameter identifications," *Mech. Time-Dependent Mater.*, vol. 18, no. 2, pp. 453–474, 2014.

[36] H. Tobushi, D. Shimada, S. Hayashi, and M. Endo, "Shape fixity and shape recovery of polyurethane shape-memory polymer foams," *Proc. Inst. Mech. Eng., L*, vol. 217, no. 2, pp. 135–143, 2003.

[37] S.-M. Lai and Y.-C. Lan, "Shape memory properties of melt-blended polylactic acid (PLA)/thermoplastic polyurethane (TPU) bio-based blends," *J. Polym. Res.*, vol. 20, no. 5, 2013, Art. no. 140.

[38] M. R. Ward, *Electrical Engineering Science*. New York, NY, USA: McGraw-Hill, 1971.

Qinglei Ji received the B.Eng. degree in aircraft design and engineering and the M.Sc. degree in engineering mechanics from the Nanjing University of Aeronautics and Astronautics, Nanjing, China, in 2015 and 2018, respectively, and the Diplôme d'Ingénieur in advanced structure and materials and the M.Sc. degree in air and ground transportation from École Nationale Supérieure de Mécanique et d'Aérotechnique, Poitiers, France, in 2018. He is currently working toward the Ph.D. degree in production engineering with the KTH Royal Institute of Technology, Stockholm, Sweden.

His research interests include additive manufacturing (3-D/4-D printing), soft robots, and microfluidics.

Mo Chen received the B.S. degree from Tongji University, Shanghai, China, in 2008, and the Ph.D. degree from Shanghai Jiao Tong University, Shanghai, China, in 2016, both in mechanical engineering.

He is currently a Researcher with the Department of Production Engineering, KTH Royal Institute of Technology, Stockholm, Sweden. His research interests include 3-D/4-D printing, especially of soft polymers and design of industrial control systems.
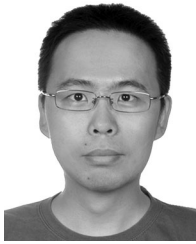
Chun Zhao received the Ph.D. degree in software engineering from Beihang University, Beijing, China, in 2017.

He is currently an Assistant Professor with Beijing Information Science and Technology University, Beijing. His research interests include the cloud manufacturing, modeling and simulation of complex systems, and Field-Programmable Gate Array (FPGA)-based cloud-edge systems.

Xiran Zhang received the B.Eng. degree in mechatronics engineering from Harbin Institute of Technology, Harbin, China, in 2018, and the M.Sc. degree in mechatronics engineering from the KTH Royal Institute of Technology, Stockholm, Sweden, in 2020.

Her research interests include 3-D/4-D printing and soft robots.
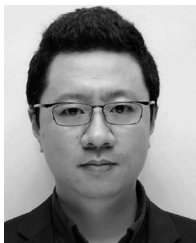
Xi (Vincent) Wang received the B.Sc. degree from Tianjin University, Tianjin, China, in 2008, and the Ph.D. degree from The University of Auckland, Auckland, New Zealand, in 2013, both in mechanical engineering.

He is currently an Associate Professor with the IIP Department of Production Engineering, KTH Royal Institute of Technology, Stockholm, Sweden. He is currently with the Division of Sustainable Manufacturing Systems (SPS). His main research interests include cloud-based manufacturing, sustainable manufacturing, robotics, computer-aided design, and manufacturing systems.

Dr. Wang is the Managing Editor for the *International Journal of Manufacturing Research*. He is also an Associate Editor for the *SME Journal of Manufacturing Systems* and the open access journal *Array* (Elsevier).

Lihui Wang received the Ph.D. degree in intelligence science from Kobe University, Japan, in 1993.

He is currently a Professor and the Chair of Sustainable Manufacturing with the KTH Royal Institute of Technology, Stockholm, Sweden. He is actively engaged in various professional activities. He has published nine books and authored in excess of 500 scientific publications. His research interests include cyber–physical systems, cloud manufacturing, real-time monitoring and control, predictive maintenance, human–robot collaborations, and adaptive and sustainable manufacturing systems.

Mr. Wang is a Fellow of the Canadian Academy of Engineering, CIRP, SME, and ASME. He is also a Professional Engineer in Canada, the President of the North American Manufacturing Research Institution of SME, and the Chairman of Swedish Production Academy. He is the Editor-in-Chief of the *International Journal of Manufacturing Research, Robotics and Computer-Integrated Manufacturing*, and *Journal of Manufacturing Systems*.

Lei Feng (Member, IEEE) received the B.Sc. and M.Sc. degrees in mechatronics from Xi'an Jiaotong University, Xi'an, China, in 1998 and 2001, respectively, and the Ph.D. degree in electrical and computer engineering from the Systems Control Group, University of Toronto, Toronto, ON, Canada, in 2007.

In 2012, he joined the Mechatronics and Embedded Control System Division, KTH Royal Institute of Technology, Stockholm, Sweden, where he is currently an Associate Professor. His main research interests include novel mechatronic systems enabled by additive manufacturing, energy management control of mechatronic systems, autonomous driving, verification and control synthesis of cyber–physical systems, and supervisory control of discrete-event systems.